

**P.Pieringer, E.Göttlich, J.Woiseschläger, W.Sanz, F.Heitmeir** (2005) *Numerical investigation of the unsteady flow through a transonic turbine stage*, Proc. 6th European Conference on Turbomachinery, Lille, pp. 339-352

# NUMERICAL INVESTIGATION OF THE UNSTEADY FLOW THROUGH A TRANSONIC TURBINE STAGE USING AN INNOVATIVE FLOW SOLVER

*P. Pieringer - E. Göttlich - J. Woisetschläger - W. Sanz - F. Heitmeir*

Institute for Thermal Turbomachinery and Machine Dynamics,  
Graz, University of Technology, Austria, paul.pieringer@tugraz.at

## ABSTRACT

In this paper a numerical investigation of the unsteady three-dimensional flow through the transonic test turbine stage at Graz University of Technology is presented. The numerical code applied solves the Reynolds-averaged Navier-Stokes equations using a time-iterative characteristic method derived by the finite-volume approach. Turbulence is modeled by the one-equation model of Spalart and Allmaras. A periodic solution is obtained by applying phase lagged boundary conditions. Wall boundary layer is simulated by pressure gradient sensitive wall functions. The effects of the tip leakage flow are considered by meshing the tip clearance between rotor blade and casing.

The results are discussed and compared with experimental data gained by time-resolved laser doppler velocimetry (LDV). Both calculation and measurements detect in good agreement the wake shedding from the trailing edges of stator and rotor blades to be phase locked to the blade passing frequency. The calculation shows, that strong shock waves periodically reflected by casing and blades are responsible for this phenomenon.

## NOMENCLATURE

$s$	entropy	$\lambda$	eigenvalue
$\vec{w}$	velocity vector	$C$	characteristic value
$p$	pressure	$\omega$	under relaxation parameter for Newton-Raphson Iteration
$c$	speed of sound	$I$	unit matrix
$\rho$	density	$\kappa_w, B_w$	constants for the wall-functions defined by Spalding (1961)
$\kappa$	ratio of specific heats	$u^+$	nondimensional parallel-to-wall velocity
$S$	cell-face area	$y^+$	nondimensional wall distance
$\nabla$	Nabla-operator	$k$	coefficient of thermal conductivity
$\vec{q}$	heat flux vector	$R$	gas constant
$\tau$	shear tensor	$\nu_l, \nu_t$	laminar and turbulent kinematic viscosity
$\xi, \eta, s$	curvilinear coordinate directions	$T$	rotor blade passing period
$i$	grid index		
$V$	cell volume		
$\vec{n}$	unit vector normal to cell face		
$\vec{e}$	unit vector of curvilinear coordinate directions		
$\vec{e}_{v1}, \vec{e}_{v2}$	unit vectors in cell face, normal to each other,	Superscript	
$\Delta$	difference operator	$T$	operator to transpose matrix

## INTRODUCTION

The design of efficient turbomachinery stages requires detailed knowledge of flow phenomena and their impact on efficiency. Nowadays turbine stages often feature three-dimensional geometrical design and high pressure ratio. So the flow is transonic and pressure shocks affect the resulting complex unsteady flow situation. Steady state CFD flow calculations capture the time averaged main flow well but lacks by definition in the predictions of unsteady effects.

The numerical calculation of the three-dimensional unsteady flow through a turbine stage holds a lot of challenges. To capture the unsteady effects the grid resolution must be fine in the whole flow domain. Boundary layer effects determine the secondary flow and the losses, so the wall boundary layer must be simulated properly. Resolving the boundary layer by a fine grid leads to small cells, which force the computational time-step value to be very small. To achieve a periodic solution a lot of blade passing periods has to be calculated. If the pitch ratio of stator and rotor is not unity, additional effort must be applied to reduce the calculation domain to one stator and rotor channel. To get appropriate results for such a problem in reasonable total computational time, a CFD solver must feature a fast algorithm, that is able to accurately solve the Navier-Stokes equations, wall-functions, that properly simulates the boundary layer to reduce total count of cells and to enable a larger time-step value, and a correct method to reduce the flow problem to one channel for stator and rotor.

The used Navier-Stokes code solves the Reynolds-averaged Navier-Stokes equation in characteristic formulation together with the one equation turbulence closure developed by Spalart and Allmaras (1994). The code requires structured grids in a multi-block arrangement. The boundary conditions are applied with phantom cells. To gain a stable and accurate procedure the code uses a decomposition of the inviscid fluxes, that are derived by the conservative formulation of the Navier-Stokes equation, leading to a set of wave-type equations (one dimensional convection equation). Using this characteristic form of the flow equations the computational efforts caused by multiple matrix manipulations of conservative flow solvers can be avoided, thus leading to reduction in computer time. The resulting scheme is not conservative for mass, momentum and energy, but the failure is negligible. Discretisation in time is done by a second-order approximation of the time evolution, which is solved in an implicit way. To cope with unequal pitch ratio, phase lagged boundary conditions (e.g. Erdos et al., 1977 and He, 1992) are applied. To further reduce calculation effort and time, pressure-gradient-sensitive wall functions were applied. Wall-functions derived by the law-of-the-wall formulation (Spalding 1961) have been suggested by Frink (1996), within this paper a new approach will be presented.

The used CFD-code was developed at the Institut for Thermal Tubomachinery in Graz by enhancements on the method sketched by Pieringer et al. (2001), so the major focus will be laid on the description of the numerical scheme.

The transonic test turbine stage at Graz University of Technology was chosen for the investigation, since a lot of experimental and numerical research has already been conducted for that test case (e.g. Göttlich et al. 2004, Pieringer et al. 2003). Experimental and numerical results will be compared, and the mechanism of phase-locked wake-shedding behind the stator trailing edge will be analyzed.

## NUMERICAL METHOD

### Discretisation in space

When using primitive variables including the entropy  $s$ , the Navier-Stokes equations can be written as follows.

$$\begin{aligned}
\frac{\partial s}{\partial t} + \bar{w} \nabla s &= \left( \frac{R}{p} \right) \left[ \nabla \bar{q} + (\tau \nabla) \bar{w} \right] \\
\frac{\partial \bar{w}}{\partial t} + (\bar{w} \nabla) \bar{w} + \frac{1}{\rho} \nabla p &= \frac{1}{\rho} (\nabla \tau)^T \\
\frac{\partial p}{\partial t} + \bar{w} \nabla p + \kappa p \nabla \bar{w} &= (\kappa - 1) \left[ \nabla \bar{q} + (\tau \nabla) \bar{w} \right]
\end{aligned} \tag{1}$$

The result of the inviscid part (Euler part) of the Navier-Stokes equations

$$\begin{aligned}
\frac{\partial s}{\partial t} + \bar{w} \nabla s &= 0 \\
\frac{\partial \bar{w}}{\partial t} + (\bar{w} \nabla) \bar{w} + \frac{1}{\rho} \nabla p &= 0 \\
\frac{\partial p}{\partial t} + \bar{w} \nabla p + \kappa p \nabla \bar{w} &= 0
\end{aligned} \tag{2}$$

can also be obtained by the solution of a set of one-dimensional characteristic equations. For a curvilinear coordinate system the characteristic equations in one index direction adopt the form

$$\frac{\partial C^\xi}{\partial t} + \lambda^\xi \frac{\partial C^\xi}{\partial \xi} = 0, \text{ and a spatially discretized form } \frac{\partial C^\xi}{\partial t} + \lambda^\xi \Delta C^\xi = 0$$

In fact the discrete equations in one index direction can be written as follows

$$\begin{aligned}
\left( \frac{\partial s}{\partial t} \right)^\xi + \frac{S^\xi}{V} (\bar{w} \bar{n}^\xi) \Delta s^\xi &= 0 \\
\left[ \frac{1}{\rho c} \left( \frac{\partial p}{\partial t} \right)^\xi + \left( \frac{\partial \bar{w}}{\partial t} \right)^\xi \bar{n}^\xi \right] + \frac{S^\xi}{V} (\bar{w} \bar{n}^\xi + c) \left[ \frac{1}{\rho c} \Delta p^\xi + \Delta \bar{w} \bar{n}^\xi \right] &= 0 \\
\left[ \frac{1}{\rho c} \left( \frac{\partial p}{\partial t} \right)^\xi - \left( \frac{\partial \bar{w}}{\partial t} \right)^\xi \bar{n}^\xi \right] + \frac{S^\xi}{V} (\bar{w} \bar{n}^\xi - c) \left[ \frac{1}{\rho c} \Delta p^\xi - \Delta \bar{w} \bar{n}^\xi \right] &= 0 \\
\left( \frac{\partial \bar{w}}{\partial t} \right)^\xi \bar{e}_{v_1}^\xi + \frac{S^\xi}{V} (\bar{w} \bar{n}^\xi) \left[ \Delta \bar{w}^\xi \bar{e}_{v_1}^\xi \right] &= 0 \\
\left( \frac{\partial \bar{w}}{\partial t} \right)^\xi \bar{e}_{v_2}^\xi + \frac{S^\xi}{V} (\bar{w} \bar{n}^\xi) \left[ \Delta \bar{w}^\xi \bar{e}_{v_2}^\xi \right] &= 0
\end{aligned} \tag{3}$$

So, the characteristic differences and the corresponding eigenvalues are

$$\begin{aligned}
\Delta C_1^\xi &= \Delta s^\xi & \lambda_1^\xi &= \frac{S^\xi}{V} \bar{w}^\xi \bar{n}^\xi \\
\Delta C_2^\xi &= \frac{1}{\rho c} \Delta p^\xi + \Delta \bar{w}^\xi \bar{n}^\xi & \lambda_2^\xi &= \frac{S^\xi}{V} (\bar{w}^\xi \bar{n}^\xi + c) \\
\Delta C_3^\xi &= \frac{1}{\rho c} \Delta p^\xi - \Delta \bar{w}^\xi \bar{n}^\xi & \lambda_3^\xi &= \frac{S^\xi}{V} (\bar{w}^\xi \bar{n}^\xi - c) \\
\Delta C_4^\xi &= \Delta \bar{w}^\xi \bar{e}_{v_1}^\xi & \lambda_4^\xi &= \frac{S^\xi}{V} \bar{w}^\xi \bar{n}^\xi \\
\Delta C_5^\xi &= \Delta \bar{w}^\xi \bar{e}_{v_2}^\xi & \lambda_5^\xi &= \frac{S^\xi}{V} \bar{w}^\xi \bar{n}^\xi
\end{aligned} \tag{4}$$

and the derivatives in time of the primitive variables can now be constructed.

$$\begin{aligned}
\frac{\partial s}{\partial t} &= -\sum_{\xi} \lambda_1^{\xi} \Delta C_1^{\xi} \\
\frac{\partial \bar{w}}{\partial t} &= -\frac{1}{2} \sum_{\xi} [(\lambda_2^{\xi} \Delta C_2^{\xi} - \lambda_3^{\xi} \Delta C_3^{\xi}) \bar{n}^{\xi} + \lambda_4^{\xi} \Delta C_4^{\xi} \bar{e}_{v1}^{\xi} + \lambda_5^{\xi} \Delta C_5^{\xi} \bar{e}_{v2}^{\xi}] \\
\frac{\partial p}{\partial t} &= -\frac{\rho c}{2} \sum_{\xi} [\lambda_2^{\xi} \Delta C_2^{\xi} - \lambda_3^{\xi} \Delta C_3^{\xi}]
\end{aligned} \tag{5}$$

To evaluate the spatial differences of the characteristics depending on the sign of the corresponding eigenvalue (upwind-discretising), a method derived from the TVD (total variation diminishing) procedure of Chakravarthy (1988) is applied, which leads to following description.

$$\begin{aligned}
\Delta C &= \Delta C_{II} \\
&+ \frac{1-\Phi}{4} \left[ \text{sign}^{23} \min \left\{ \text{abs}(\Delta C_{II}), \text{abs} \left( \frac{3-\Phi}{1-\Phi} \Delta C_{III} \right) \right\} - \text{sign}^{12} \min \left\{ \text{abs}(\Delta C_I), \text{abs} \left( \frac{3-\Phi}{1-\Phi} \Delta C_{II} \right) \right\} \right] \\
&+ \frac{1+\Phi}{4} \left[ \text{sign}^{23} \min \left\{ \text{abs}(\Delta C_{III}), \text{abs} \left( \frac{3-\Phi}{1-\Phi} \Delta C_{II} \right) \right\} - \text{sign}^{12} \min \left\{ \text{abs}(\Delta C_{II}), \text{abs} \left( \frac{3-\Phi}{1-\Phi} \Delta C_I \right) \right\} \right]
\end{aligned} \tag{6}$$

Depending on the sign of the corresponding eigenvalue  $\lambda$ , the spatial differences  $\Delta C_I$ ,  $\Delta C_{II}$  and  $\Delta C_{III}$  and the two values  $\text{sign}^{12}$  and  $\text{sign}^{23}$ , depending on the sign of the spatial differences must be set.

$$\begin{aligned}
\lambda > 0 &\rightarrow \Delta C_I = C_{i-1} - C_{i-2} \quad \Delta C_{II} = C_i - C_{i-1} \quad \Delta C_{III} = C_{i+1} - C_i \\
\lambda < 0 &\rightarrow \Delta C_I = C_{i+2} - C_{i+1} \quad \Delta C_{II} = C_{i+1} - C_i \quad \Delta C_{III} = C_i - C_{i-1}
\end{aligned} \tag{7}$$

$$\text{sign}^{12} = \frac{1}{2} [\text{sign}(\Delta C_I) + \text{sign}(\Delta C_{II})], \quad \text{sign}^{23} = \frac{1}{2} [\text{sign}(\Delta C_{II}) + \text{sign}(\Delta C_{III})] \tag{8}$$

When choosing  $\Phi = 1/3$ , this algorithm leads to a stable approximation of spatial third order accuracy.

The viscous terms were constructed in a central-differencing manner, and superposed to the Euler results.

### Discretisation in time

The parabolical approximation of the time-derivatives leads to the implicit condition

$$\frac{3}{2} q^{t+1} - \frac{4}{2} q^t + \frac{1}{2} q^{t-1} \approx \Delta t \left( \frac{\partial q}{\partial t} \right)^{t+1} \tag{9}$$

which is solved using the Newton-Raphson method,

$$\left( \frac{3}{2} I - \Delta t \frac{\partial \left( \frac{\partial q}{\partial t} \right)^n}{\partial q} \right) \Delta q^n = \left[ - \left( \frac{3}{2} q^n - \frac{4}{2} q^t + \frac{1}{2} q^{t-1} \right) + \Delta t \left( \frac{\partial q}{\partial t} \right)^n \right] \omega \quad \text{and} \quad q^{n+1} = q^n + \Delta q^n \tag{10}$$

driving  $q^n$  for  $n \rightarrow \infty$  to the value  $q^{t+1}$ . Instead of starting the Newton-Raphson iteration with  $q^n = q^t$  for  $n=0$ , the starting values were determined by an approximation on a coarser grid. After transposing the flow problem to a coarser grid ( $q^t \rightarrow Q^t$ ), it is solved first order accurate in time and space ( $Q^{t+1}$ ), and the results were used for the initialization on the fine grid,  $q^n = q^t + Q^{t+1} - Q^t$  for  $n=0$ . The propagation of low frequency disturbance, that can be predicted very well by a coarser grid, is well captured by this method, and a reduced count of Newton-Raphson steps on the fine grid is sufficient for convergence.

### Phase-lagged boundary conditions

To gain periodic solutions in time and space for arbitrary stator and rotor blade numbers, phase lagged boundary conditions at geometrical periodic boundaries and at the interface between stator and rotor domain were applied. A direct-store technique is used, the updates on the boundaries is done by a weighted average of the newly available flow-field and the stored variables. To keep the demand of computer memory low, not each but a sufficient amount of time-step values is stored and a linear interpolation is used for the reconstruction of the boundary values.

### Pressure-gradient-sensitive wall function

The applied wall-function is based on the law-of-the-wall formulation by Spalding (1961) and considers the shear-stress distribution perpendicular to the wall surface, which is mainly determined by pressure gradients (Pieringer, 2005). This wall function assumes steady state conditions.

The law-of-the-wall formulation by Spalding (which was slightly modified for this wall-function approach) describes the non-dimensional parallel to the wall velocity distribution of a turbulent boundary layer for zero pressure gradient flows. (The direction of  $y$  is normal to the wall.)

$$y^+ = u^+ + e^{-\kappa_w B_w} \left[ e^{\kappa_w u^+} - 1 - \kappa_w u^+ - \frac{(\kappa_w u^+)^2}{2} - \frac{(\kappa_w u^+)^3}{6} - \frac{(\kappa_w u^+)^4}{24} \right] \quad (11)$$

The assumption, that within the boundary layer the shear stress is constant, leads to an equation for the ratio of turbulent and laminar kinematic viscosity.

$$\frac{\nu_t}{\nu_l} = e^{-\kappa_w B_w} \left[ e^{\kappa_w u^+} - 1 - \kappa_w u^+ - \frac{(\kappa_w u^+)^2}{2} - \frac{(\kappa_w u^+)^3}{6} \right] \quad (12)$$

By knowing the parallel to the wall velocity at a point with a defined distance to the wall and estimating the laminar viscosity and the density at the wall, one can figure out the distribution of the parallel velocity and the ratio of turbulent and laminar kinematic viscosity between that point and the wall. By using phantom cells to impose the boundary condition, an easy way is to take all known values of the first calculation cell close to the wall and to calculate the values of the phantom cells, having a defined distance to the wall. So there is a clearance between the first calculation cell and the wall.

When pressure gradients occur, the assumption, that within the boundary layer the shear stress is constant, is not valid anymore. Close to a wall the shear stress will rather be a function of skin-friction, distance to wall and pressure gradients parallel to the wall. In fact the equilibrium of forces predicts

$$\rho(\nu_l + \nu_t) \frac{\partial u}{\partial y} = \tau_{xy}(y) \approx \tau_{xy}(0) + y \frac{\partial p}{\partial x} \quad (13)$$

By scaling the spatial distribution of the ratio of laminar and turbulent viscosity, that can be derived by Eq. (12) and Eq. (11), to hit the local available value at the position of the first calculation cell, Eq. (13) defines the spatial derivative of the velocity  $u$ . Since  $u$  is zero at the wall and has to adopt the known value at the first calculation cell the velocity profile and the skin-friction can be calculated. Now the velocity profile is used to define the velocity in the phantom cell and the scaled distribution of the ratio of laminar and turbulent viscosity is used to define the Spalart Allmaras turbulence variable there (for detailed description see Pieringer, 2005).

For three-dimensional problems, the pressure gradients in two perpendicular directions parallel two the wall are needed in order to properly define the boundary layer. In the phantom cell the velocity perpendicular to the wall surface is set to zero and the pressure is extrapolated from the calculation domain.

When postulating adiabatic wall condition, the equilibrium of heat flow and work by shear forces,

$$k \frac{\partial T}{\partial y} + u\rho(v_i + v_t) \frac{\partial u}{\partial y} = 0 \quad (14)$$

derived by the fact, that energy-flux towards the wall must be equal zero, holds at the wall and also within the boundary layer. Therefore Eq. (14) is used to calculate the temperature of the phantom cell.

Since this boundary layer approximation is derived from steady-state conditions, some additional error will occur by applying it to time-resolved calculations.

## VALIDATION

To validate the presented numerical scheme the blade VKI LS 59 was chosen for comparison to the TTM solver, a flow-solver that is based on conventional and well established schemes.

The TTM solver solves the Reynolds-averaged Navier-Stokes equations by means of a fully-implicit time-marching finite-volume method and is described in detail by Gehrler (1999). The governing equations are treated in conservative form, the convective parts are discretized using a third-order-accurate TVD-upwind scheme, based on the MUSCL type of an upwind scheme.

The VKI LS 59 is modeled 3D with span 0.1m. The mesh for the TTM solver is designed for resolving the boundary layer at the wall, leading to a cell count of about 400.000. For the presented numerical scheme the mesh is designed for simulating the boundary layer at the wall using the presented wall function, leading to a cell count of about 240.000. Besides from boundary layer area both grids do not differ from the other.

At the inlet total pressure  $p_t = 1.413$  bar and total temperature  $T_t = 308.0$  K and at the outlet isentropic Mach number  $M_{is} = 0.7$  are applied, turbulence is modeled by Spalart Allmaras turbulence closure.

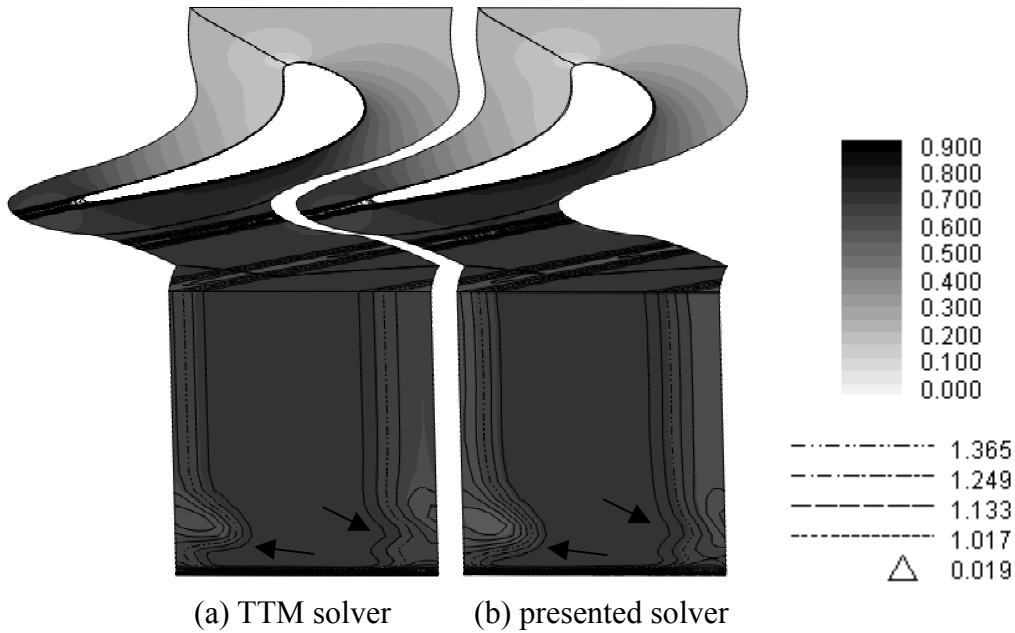


**Fig. 1:** VKI LS 59, grayscale indicates Mach number, lines indicate total pressure

Results at mid-span and outlet (Fig.1) show, that there is excellent agreement in Mach number (Fig. 1, grayscale) and well agreement in total pressure (Fig. 1, lines). There are only minor deviations in total pressure close to the casing (Fig.1, arrows).

Apart from time-saving due to the reduced amount of necessary computational grid-cells, the presented solver needed half the time for discretising the Euler-parts of the Navier-Stokes equations at each cell compared to the TTM solver, this further reduced computational time.

## TEST CASE

The transonic test turbine stage at Graz University of Technology is a cold flow test turbine facility (Erhard and Gehrler, 2000), which is a unique combination of a max. 2.8 MW axial test turbine and a directly coupled compressor that generates more than half of the compressed air needed to drive the turbine. To cover the losses additional air is provided by a separate, electrically driven compressor station. The turbine casing allows access for conventional as well as optical measurement devices.

The test turbine stage contains 24 stator blades and 36 rotor blades, which leads to a pitch ratio of 2/3. Whereas the inner diameter of the stage is constant ( $D = 0.4$  m) the outer casing shows a converging-diverging contour. The minimum of the flow channel height is at the aft section of the stator ( $D_{\min} = 0.503$  m), then the outer contour is a cone with an opening angle of  $12^\circ$  ( $D_{\text{outlet}} = 0.553$  m). The design exit angle of the stator is  $69.7^\circ$  from the axis. The gap between the rotor blades and the casing is  $0.95$  mm, which is 1.56% of the blade height at the leading edge and 1.36% of the blade height at the trailing edge.

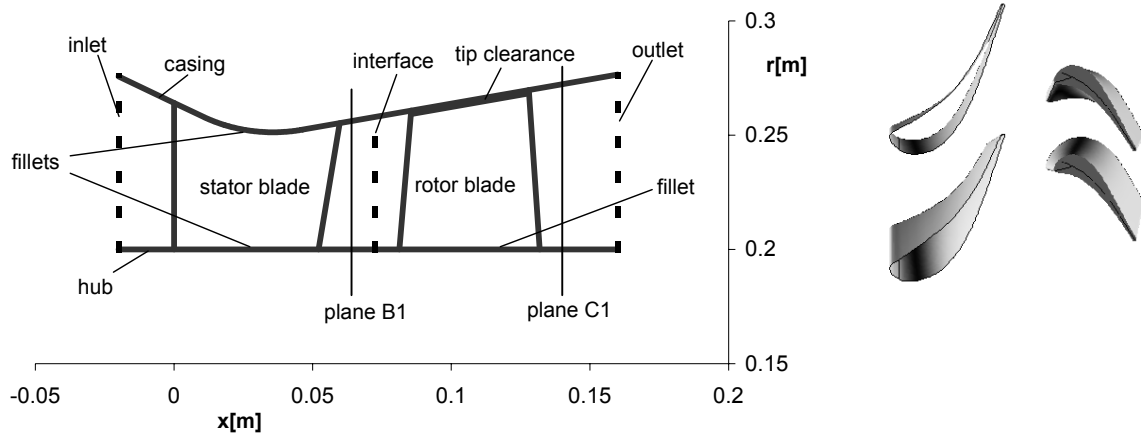


**Fig. 2:** Transonic test turbine stage at Graz University of Technology, geometry overview

## Computational Grid

A multi-block grid consisting of 10 blocks and a total count of about 1.000.000 cells is used for the numerical calculation.

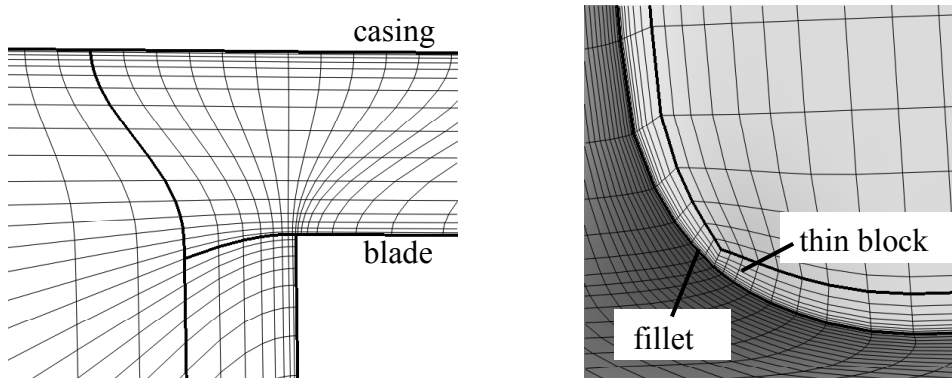


**Fig. 3:** Grid details, left: tip-clearance of the rotor-blade, right: meshing of the fillets

The tip clearance between rotor blade and outer casing is meshed by (only) 16 cells, though the use of wall-functions still allows a good spatial resolution there (Fig. 3, left). The fillets at the stator hub and tip and at the rotor hub are modeled as well. To prevent singularities there, a thin block covers the wall domain at the blades (Fig. 3, right). The channel is meshed by 72 cells from hub to outer casing.

## Boundary Conditions

### Inlet Boundary Conditions:

total pressure: 3.4202 bar

total temperature: 403.0° K

inlet angle: 0° (peripheral)

Spalart-Allmaras turbulence variable:  $\tilde{\nu}/\nu_t = 0.1$

The Spalart-Allmaras turbulence model was designed for fully turbulent flow with low free-stream turbulence. As the turbulence intensity at the inlet was not known, the value for  $\tilde{\nu}/\nu_t$  was set to 0.1, which is a suggested value by Spalart and Allmaras (1994) for low free-stream turbulence.

### Outlet Boundary Conditions:

static pressure: 0.935 bar

number of revs: 10545.5 rpm.

## Calculation Parameters

A steady-state solution was achieved by using a mixing plane technique between stator and rotor. Two-dimensional non-reflecting boundary conditions using the circumferentially averaged static pressure at the rotor inlet were applied at the stator outlet. The flow angle, the total pressure and the total temperature extracted from the circumferentially averaged values at the outlet of the stator grid determined the inlet of the rotor grid.

Starting from the steady state result 30.000 time steps with a value  $\Delta t = 1.7561e-7$  sec were calculated to obtain a periodic unsteady solution. The maximum CFL number was about 7. One stator period lasts 900 time steps and one rotor period lasts 1350 time steps, so more than 33 stator periods and 22 rotor periods were computed. The approximation on the coarser grid (every second grid-point) for each time step was calculated first-order accurate in time and space. Afterwards on the fine grid each time step was solved by 6 Newton-Raphson steps with an under-relaxation value of  $\omega = 0.6$ . On the fine grid the nondimensional wall distance  $y^+$  was below 80 at each cell close to a wall. For the phase-lagged boundary condition every 6<sup>th</sup> time step was stored, getting a resolution of 150 stored value-sets for the stator and 225 for the rotor. The weighting factor for the updates was set to 0.7. The calculation time was about four weeks on a modern 1.25 GHz, 64-bit computer.

The calculation parameters were tested by a quasi 3D investigation of the presented test case. Brilliant agreement for multi-passage (two stator channels, three rotor channel) and phase-lagged (one channel each) results was achieved, proving the valid application of the phase-lagged boundary conditions in terms of method and parameters for that test case.

## MEASUREMENT SETUP

The optical velocity measurements of the flow were performed using a two-dimensional LDV-system (Göttlich et al. 2004). Optical access was realized through a small glass window, to gain the axial and circumferential velocity. The data were recorded in five axial planes by point-wise detection along radial lines, circumferential traversing was achieved by turning the stator-casing. To allow a rotor-phase-resolved analysis of the measured velocities, a reference signal provided by the monitoring system of the turbine was used to trigger the data sampling.

The data of two planes were used to compare with the numerical results, plane B1 is located close behind the trailing edge of the stator and plane C1 is located close behind the rotor (Fig. 2 and Fig. 4).

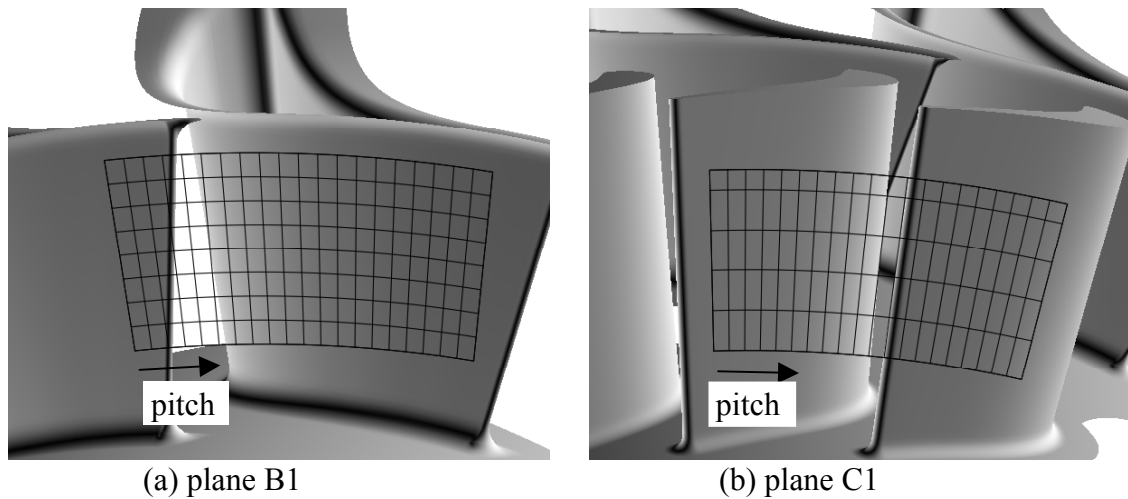


**Fig. 4:** Measurement grid

## RESULTS

### Comparison of Measured and Calculated Data

The comparison of measured and calculated data is performed by evaluating the time-pitch plot and the time-span plot of axial and circumferential (against pitch-wise direction) velocity.

#### Plane B1

The time-pitch plot in plane B1 at 54% span points out a shock-wave that strongly alters the circumferential velocity (Fig.5, mark A). The measurements and the CFD results disagree in its position, but both show the shock-position to be almost time independent.

In the wake (Fig.5, mark B) vortex structures can be detected. The wake is showing phase locked wake shedding that must be periodically triggered. The measurements show seven vortices a period, the CFD results six. The wake is slightly deflected in pitch-wise direction at about  $t/T = 0.5$  for CFD and  $t/T = 0.4$  for measurements.

Periodically a shock-wave crosses the evaluation domain (Fig.5, mark C) and a significant stronger vortex in the wake can be detected after that in the measurements and in CFD results (Fig.5, mark D). The CFD results capture both phenomena well, but they are time-delayed compared to the measurements.

The axial velocity shown in the time-span plot of a radial line positioned at pitch 0.3 (within the wake) indicates cylindrical vortex shedding in CFD results (Fig. 6(a)), the measurements detect the breakup of that cylindrical behavior by an additional vortex below span 30% (Fig. 6(b), arrow). The axial velocity decrease (Fig. 6, mark A), that is well predicted in CFD results but time delayed compared to the measurements, indicates that the triggering mechanism of the wake shedding differs in span position.

Further investigations have to be carried out to detect the reasons for the time delay of the numerical results.

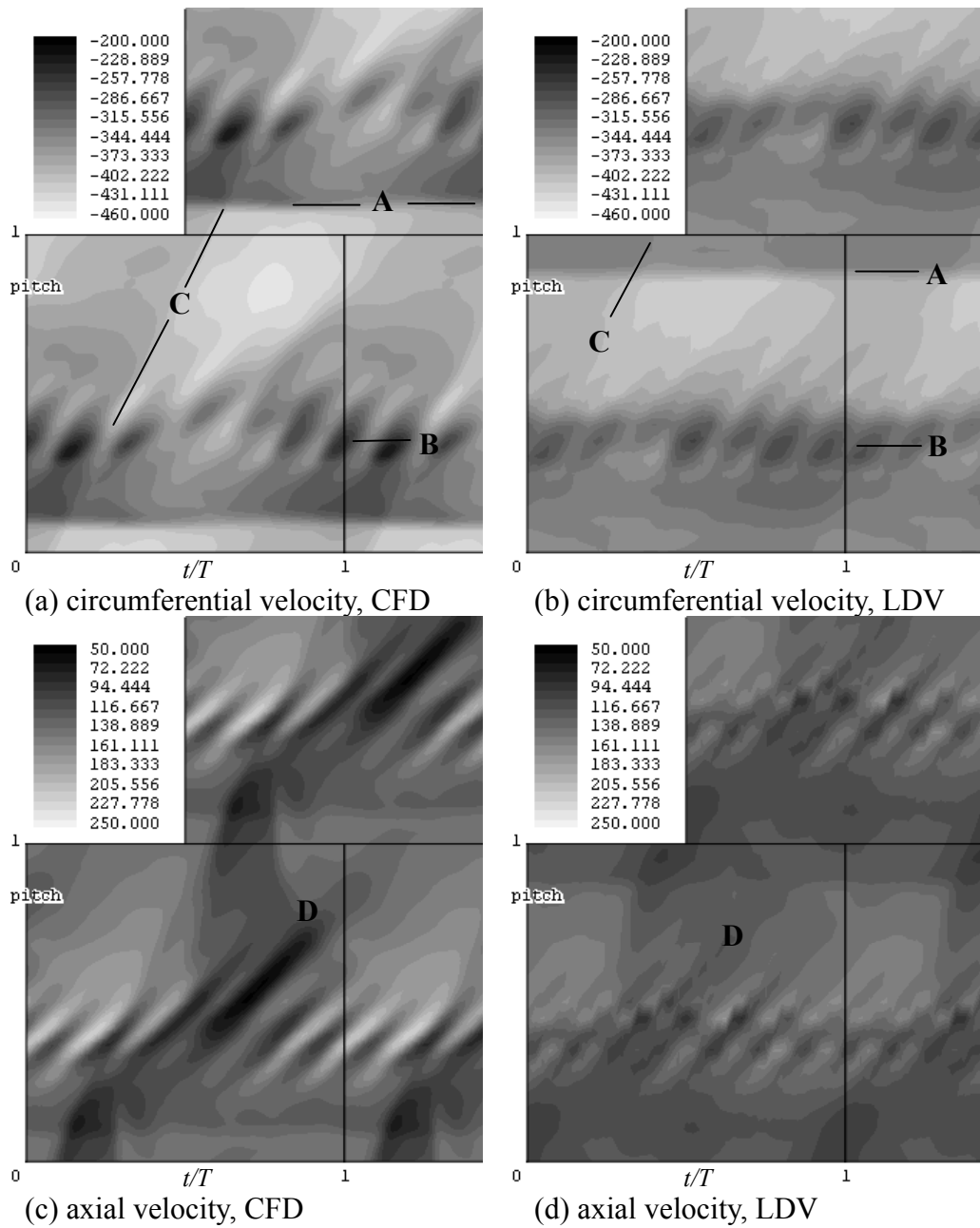


**Figure 5:** Plane B1, at 54% span

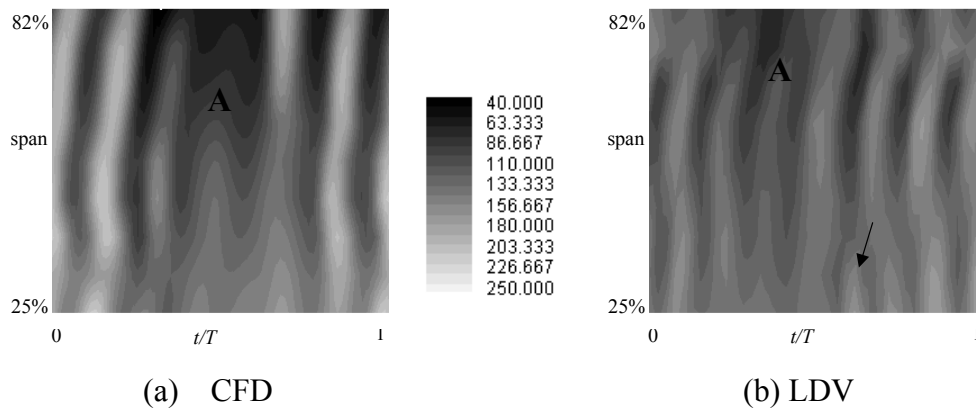


**Figure 6:** Plane B1, at 0.3 pitch, axial velocity

Plane C1

The absolute-frame point of view causes all effects, that refer to the moving position of the rotor blade, to be inclined. The time-pitch plot (the pitch still represents the stator pitch) in plane C1 at 53% span shows as well phase-locked wake shedding (Fig.7, mark A) behind the rotor trailing edge. Both, measurements and CFD results show nine vortices per one stator blade passing period. There is some periodic increase of the axial velocity component within the wake in good agreement between CFD results and measurements (Fig.7, marked with a white circle), but no strong shock wave can be detected, to cause the phase locking of the vortex shedding.

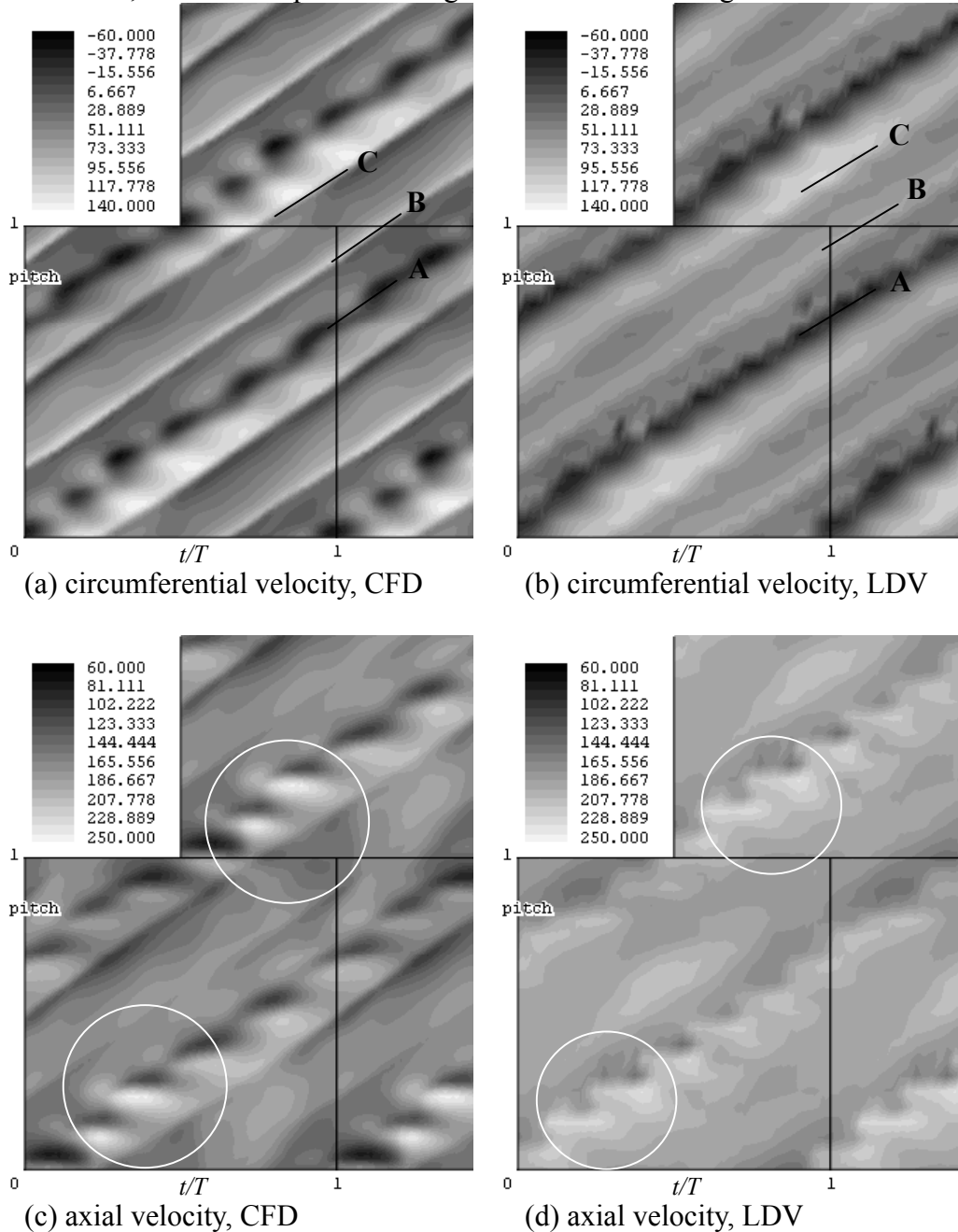


**Figure 7:** Plane C1, at 53% span

The circumferential velocity plots show furthermore the position of the suction side trailing edge shock (Fig.7, mark B), and another one (Fig.7, mark C), that is assumed to be the reflection of the pressure side trailing edge shock of the neighboring blade, being reflected at the aft section of the suction side. In good agreement of CFD results and measurements the positions of these shocks are very much time-independent referring to the moving rotor blade.

### Wake Shedding Triggering Mechanism at the Stator Trailing Edge

The suction side shock extends across the interface towards the rotor blade (Fig.8, fat line at  $t/T = 0.14$ , and Fig. 5, mark A), being periodically reflected. This reflected shock wave moves back again towards the suction side of the stator blade (Fig.8, dashed line and Fig.5, mark C) and impinges on the trailing edge (Fig.8,  $t/T = 0.28$ ). There it forces the wake to a vortex-separation (Fig. 8, arrow). From then on the wake shedding is undisturbed, until the next reflected shock wave triggers a vortex again.

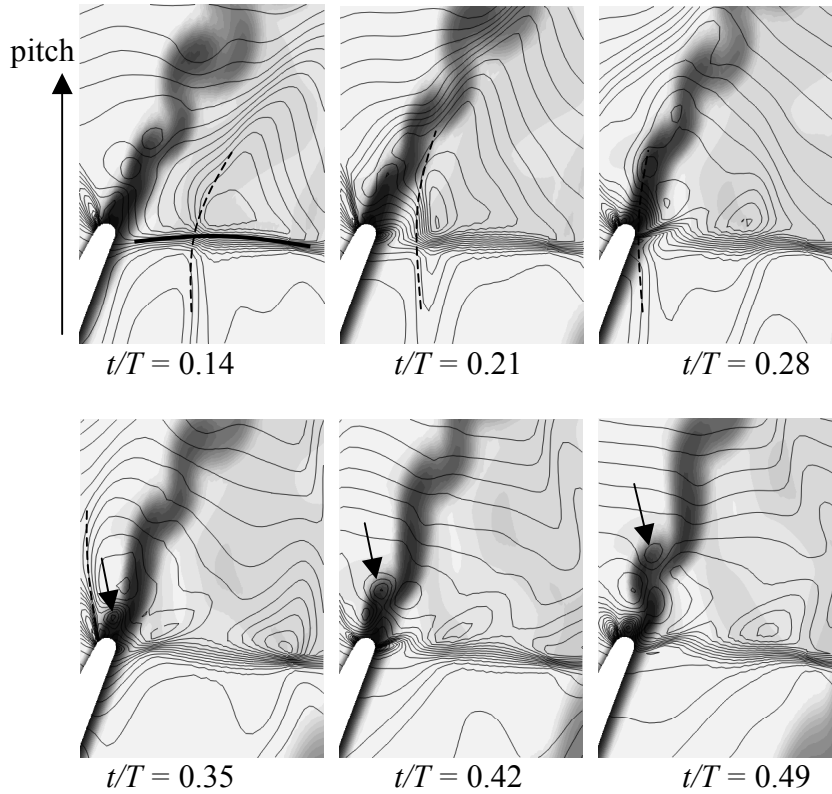


**Figure 8:** Stator wake at 50% span, lines indicate isobars, grayscale indicates entropy

### Comparison of Time Resolved and Steady State Calculation

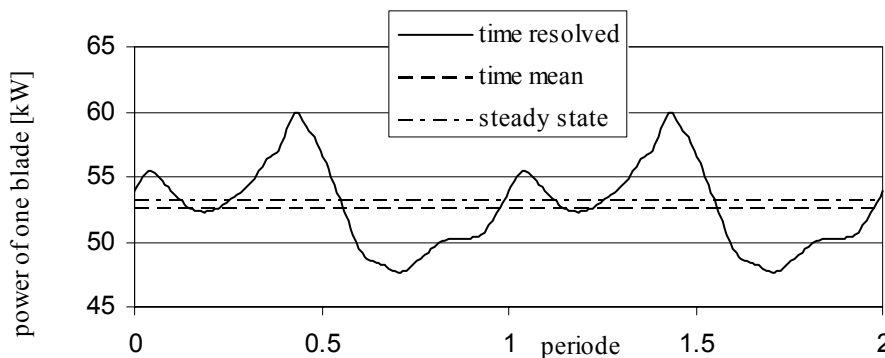


**Figure 9:** Power of one blade

The time resolved power of one blade (Fig. 9) shows two peaks a period and 24% peak-to-peak value referring to the time mean value. The steady state calculation overestimates the power by 1.1% compared to the time mean value.

The entropy distribution behind the stator trailing edge shows a distinct wake for the steady state calculation (Fig.10, left, dashed line), whereas the time mean of the unsteady calculation shows an

extension of the influence domain by the wake to about 2/3 of the whole channel, due to the vortex shedding. The position of the trailing edge shock, indicated by a sharp entropy rise, is very the same for the steady state calculation and the time mean of the unsteady calculation (Fig.10, arrow).

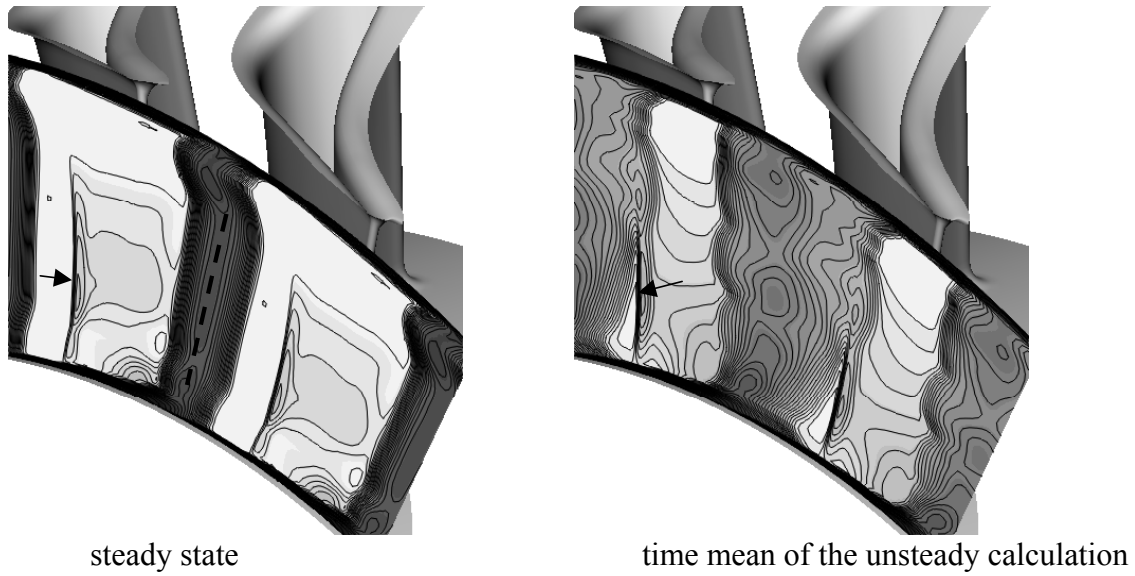


**Figure 10:** Stator exit flow, grayscale and lines indicate entropy

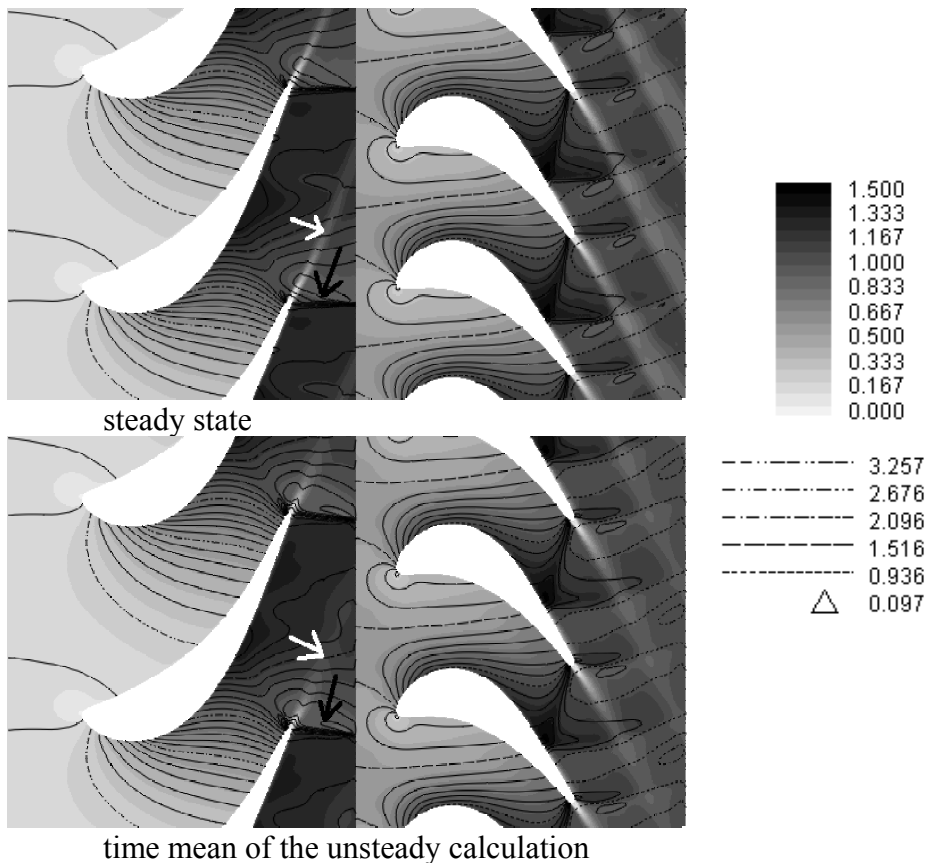


**Figure 11:** Flow at radius 0.225 m (about mid-span), grayscale indicates relative Mach number, lines indicate pressure

Figure 11 shows the flow field of the steady state and the time mean of the unsteady calculation at about mid-span. There is very well agreement in terms of Mach number and pressure for stator and rotor domain, apart from the stator wake (Fig.11, white arrow), that is smoothed by the

unsteady calculation, and the stator trailing edge shock (Fig.11, black arrow) that is slightly stronger predicted by the steady state calculation. Nevertheless the steady state calculation is very capable of predicting the time mean flow.

## CONCLUSIONS

A numerical study of the three-dimensional unsteady flow through a transonic turbine stage was carried out using an innovative flow solver.

The code is based on the characteristic flow equations to avoid time consuming matrix manipulations necessary for conservative solvers, thus leading to a fast algorithm. To further reduce computer time a novel approach for a boundary-layer simulating wall-function was introduced, that considers the influence of the pressure gradients on the shear-stress distribution perpendicular to the wall surface. To gain periodic solutions in time and space, phase lagged boundary conditions at geometrical periodic boundaries and at the interface between stator and rotor domain were applied.

By comparison with measurement data the numerical method proved to predict the unsteady three-dimensional effects well, though some disagreements could be detected. The phenomenon of phase locked wake shedding could be verified by CFD results and its mechanism behind the stator trailing edge could be described. The suction side trailing edge shock wave of the stator proves to be responsible for that phenomenon. The shock wave periodically hits the rotor suction side, and the reflection moves back to the stator trailing edge, triggering the vortex shedding.

## REFERENCES

- Chakravarthy S.R.** (1988) *High Resolution Upwind Formulations for the Navier-Stokes Equations*, VKI Lecture Series 1988-5, Computational Fluid Dynamics
- Erdos J, Alzner E, McNally W,** (1977) *Numerical Solution of Periodic Transonic Flow Through a Fan Stage*, AIAA Journal, Vol. 15, no. 11, 1559-1568
- Erhard J, Gehrler A** (2000) *Design and Construction of a Transonic Test-Turbine Facility*, ASME Paper 2000-GT-0480, International Gas Turbine and Aeroengine Congress
- Frink N,** (1996) *Assessment of an Unstructured-Grid Method for Predicting 3-D Turbulent Viscous Flows*, AIAA Paper 96-0292
- Göttlich E, Neumayer F, Woissetschläger J, Sanz W, Heitmeier F** (2004), *Investigation of Stator-Rotor Interaction in a Transonic Turbine Stage Using Laser Doppler Velocimetry and Pneumatic Probes*, ASME Journal of Turbomachinery, Vol. 126, 297-305
- He L** (1992), *An Euler Solution for Unsteady Flows Around Oscillating Blades*, ASME Journal of Turbomachinery, Vol. 112, 714-722
- Pieringer P, Gehrler A, Sanz W** (2001), *Calculation of Stator-Rotor Interaction of a Transonic Turbine Stage Using an Innovative Unsteady Flow Solver*, Proceedings of the 4<sup>th</sup> European Conference on Turbomachinery, Firenze, 1009-1020
- Pieringer P, Sanz W, Neumayer F, Gehrler A, Heitmeier F** (2003), *Numerical Investigation of the Three-Dimensional Flow Through a Transonic Turbine Stage*, Proceedings of the 5<sup>th</sup> European Conference on Turbomachinery, Prag, 1115-1131
- Pieringer P, Sanz W** (2005), *A Pressure-Gradient-Sensitive Wall Function for the Prediction of Turbulent Flow in Thermal Turbomachinery*, GT2005-68471, accepted at the ASME Turbo Expo 2005
- Gehrler A.** (1999), *Entwicklung eines 3D-Navier-Stokes Codes zur numerischen Berechnung der Turbomaschinenströmung*, Doctoral Thesis, Graz, University of Technology
- Spalart P.R., Allmaras S.R.,** (1994), *A One Equation Turbulence Model for Aerodynamic Flows*, La Recherche Aérospatiale, No.1, 5-21
- Spalding D.B.** (1961), *A Single Formula for the Law of the Wall*, Trans ASME Series A, J Appl Mech vol28, no 3, pp 444-458